Journal Name

ARTICLE TYPE

Cite this: DOI: 10.1039/xxxxxxxxxx

Magnetite-supported palladium single-atoms do not catalyse the hydrogenation of alkenes but small clusters do†

Marta D. Rossell,*[a] Francisco J. Caparrós,[b] Inmaculada Angurell,*[b] Guillermo Muller,[b] Jordi Llorca,[c] Miquel Seco,[b] and Oriol Rossell[b]

Received Date
Accepted Date

DOI: 10.1039/xxxxxxxxxx

www.rsc.org/journalname

The activity of supported noble metal catalysts strongly depends on the particle size. The ultimate small-size limit is the single-atom catalyst (SAC), which is known to maximize the catalytic efficiency. Here, we investigate the catalytic behavior of Pd SACs supported on magnetite nanoparticles and, in clear contrast with all reports, we demonstrate that Pd SACs are absolutely inactive in the hydrogenation of various alkene substrates. Instead, Pd clusters of low atomicity exhibit outstanding catalytic performances.

Supported noble metal catalysts have received tremendous attention in the last years[1] because of their high activity and selectivity for a large number of reactions. In this context, functionalized magnetic nanoparticles have emerged as viable supporting materials given that they offer the advantage of being easily separable from the reaction solution by an external magnet.[2] This is important in order to prevent loss of catalyst and, at the same time, to increase its reusability.[3] For the fabrication of these systems noble metals are dispersed finely on the magnetite support and the size of the metal particles becomes a crucial factor that governs the performance of the catalyst.[4] It is well known that generally subnanometre clusters have better catalytic activity and/or selectivity than nanometre-sized nanoparticles, most probably due to the low coordination of the unsaturated atoms that act as active sites.[5] The lowest limit of downsizing metal particles is to disperse the metal exclusively as isolated atoms, denoted as "single-atom catalyst" (SAC). SACs are desirable species because, potentially, all the atoms are able to catalyse. This property has also important economic implications. But the question that arises is whether isolated single atoms have a better performance than the corresponding sub- or nanometre-sized particles. The answer is yes for the vast majority of examples, such as the water-gas shift reaction (WGS), CO oxidation and preferential oxidation (PROX) of CO in H_2,[6,7] methane conversion,[8] and other reactions.[9–11] This general concept is challenged by recent studies on Au-based catalysts. Specifically, Corma showed that Au SACs accompanied with Au dimers supported on functionalized carbon nanotubes presented an initial induction period in the aerobic oxidation of thiophenol with O_2,[12] suggesting that the active species were not the isolated gold atoms present but other metal species formed during the reaction. In order to clarify this scenario, we have investigated the catalytic performance of Pd SACs and/or nanoclusters supported on magnetite nanoparticles for the hydrogenation of styrene. Surprisingly, we have found that Pd SACs are not active at all in the hydrogenation of styrene. Besides, the individual atoms of Pd anchored on the Fe_3O_4 support were recovered unaltered and no metal aggregation was detected. These facts permit to establish unambiguously that Pd SACs supported on magnetite do not catalyse the hydrogenation of styrene. This behaviour contradicts the excellent catalytic efficiency described for Pd SACs in the following processes: carbon monoxide oxidation,[13] hydrogenation of alkynes and nitroarenes,[14] selective aerobic oxidation of allyl alcohols,[15] selective hydrogenation of 1,3-butadiene,[16] and hydrogenation of styrene and acetylene on Cu metal surface.[17] However, it should be noted that for the reactions investigated in the preceding examples, the nature of the supporting surface as well as the reaction conditions are clearly different from those described here. In this paper, we have distinctly proven that while the single isolated Pd atoms are utterly inactive, nanoclusters of 0.9-1.5 nm display prominent TOFs

[a] *Electron Microscopy Center, Empa, Swiss Federal Laboratories for Materials Science and Technology, Überlandstrasse 129, 8600 Dübendorf, Switzerland. E-mail: marta.rossell@empa.ch*
[b] *Departament de Química Inorgànica, Universitat de Barcelona (UB), Martí i Franquès 1-11, 08028 Barcelona, Spain. E-mail: inmaculada.angurell@qi.ub.es*
[c] *Institut de Tècniques Energètiques i Centre de Recerca en Nanoenginyeria, Universitat Politècnica de Catalunya (UPC), Diagonal 647, 08028 Barcelona, Spain*

† Electronic Supplementary Information (ESI) available. See DOI: 10.1039/b000000x/

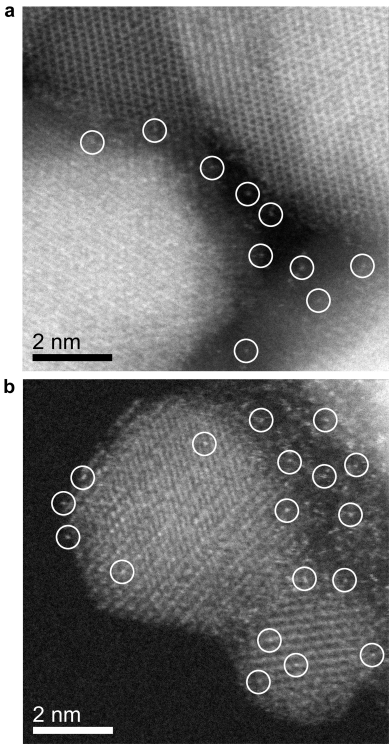

Fig. 1 HAADF-STEM images of sample 1. (a,b) Examination of different regions reveal isolated Pd atoms (white circles) uniformly dispersed on the magnetite support. For clarity, only a few isolated Pd atoms are encircled in each panel, although many more are present.

for the hydrogenation of styrene that significantly exceed the best reported results for supported Pd catalysts.

The deposition of metals on the magnetic nanoparticles can be achieved by the direct reaction of the metal precursor salts with bare magnetic nanoparticles followed by reduction. This strategy generally provides poor nanoparticle size distributions so that it is preferable to previously functionalize the magnetite nanoparticles with linkers equipped with terminal coordinating groups.[18] We have taken advantage of our method based on the use of the auxiliary ligand $dopPPh_2$,[19] which contains a catechol moiety able to anchor to the magnetite surface. Pd loading onto $Fe_3O_4dopPPh_2$ nanoparticles involves the addition of the appropriate amount of $K_2[PdCl_4]$ to a previously sonicated suspension of $Fe_3O_4dopPPh_2$ in water, followed by reduction with $NaBH_4$. The total Pd deposited was obtained by inductively coupled plasma optical emission spectrometry (ICPoes). To evaluate the effect of Pd loading on the structure and performance of the final catalyst we prepared five samples of NPs containing a Pd weight content of 0.18% (sample 1), 0.38% (sample 2), 0.63% (sample 3), 0.90% (sample 4), and 3.48% (sample 5) for catalytic tests. All the samples were investigated by high-angle annular dark-field scanning transmission electron microscopy (HAADF-STEM). This technique, also known as *Z-contrast imaging*, has a high atomic number sensitivity approaching the Rutherford cross section (proportional to Z^2). Thus, the heavy Pd species can readily be detected with brighter contrast on the magnetite support. Representative HAADF-STEM images of sample 1 show that all Pd species exist exclusively as isolated single atoms; neither subnanometre clusters nor nanoparticles are detected by an exhaustive analysis (Fig. 1). In contrast, images of sample 2 reveal the presence of only a few isolated Pd atoms along with small particles in the range of 0.9-1.5 nm (Fig. 2a and b). Images of samples 3-5 show nanoparticles, whose size increases with Pd content (Fig. 3).

Surface analysis by X-ray photoelectron spectroscopy (XPS) shows Pd/Fe atomic ratios of 0.016, 0.021 and 0.025 for samples 2 to 4, respectively. Interestingly, the surface Pd/Fe atomic ratio normalized by the Pd content progressively decreases as the Pd content increases, which provides further evidence of the progressive formation of Pd clusters and nanoparticles following an increase of the Pd content. The Pd signal in sample 1 is quite low due to the low metal content of the sample and it is not possible to accurately determine the Pd/Fe ratio. In accordance to the HAADF-SEM results, the binding energies recorded in samples 1 and 2 for Pd $3d_{5/2}$ and Pd $3d_{3/2}$ at 337.9-337.2 and 342.3-342.5 eV, respectively (see Fig. 4) are typical for ionic Pd and small Pd nanoclusters.[20] In the XP spectra of samples 3 and 4, in addition to these photoelectrons, there is another component corre-

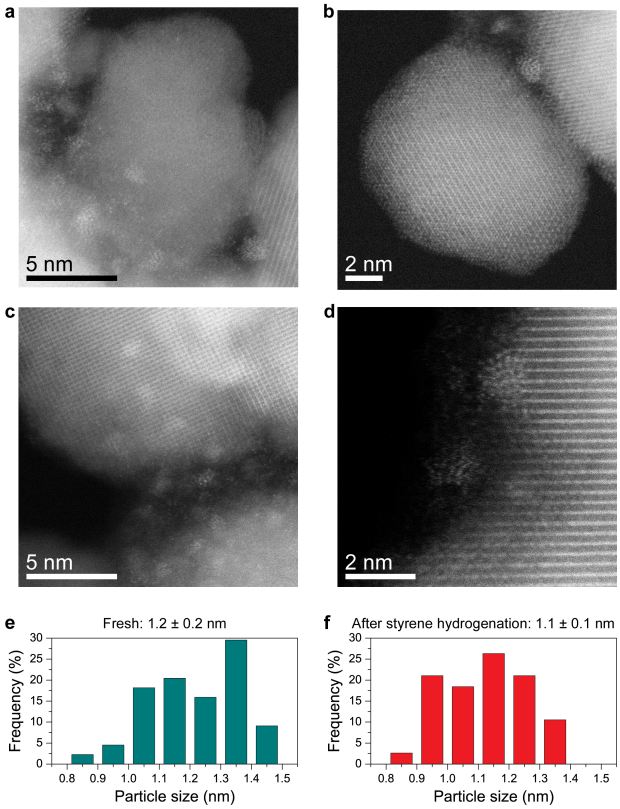

Fig. 2 HAADF-STEM images of sample 2. The dispersion and distribution of Pd on the catalyst was studied before and after two styrene hydrogenation reaction cycles. (a,b) Two different images of the fresh sample evidencing the presence of Pd nanoparticles with diameters <1.5 nm (seen with enhanced contrast). (c,d) In the reacted sample, Pd clusters of comparable sizes are observed indicating that no sintering has occurred. (e,f) Comparison of the Pd particle size distribution calculated for sample 2 before and after the styrene reactions.

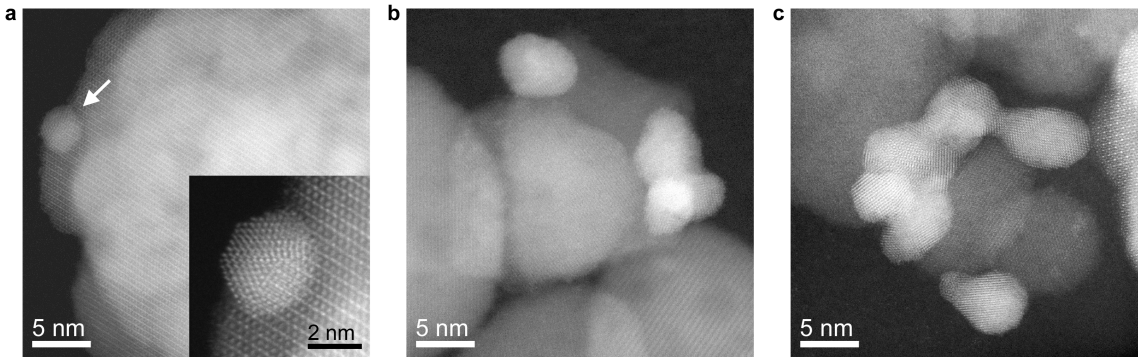

Fig. 3 HAADF-STEM images of samples 3-5. Pd nanoparticles with sizes >3 nm are clearly visible with enhanced contrast on the magnetite support. The amount and the diameter of the Pd particles increase with Pd weight content: (a) 0.63% (sample 3); (b) 0.90% (sample 4); (c) 3.48% (sample 5). The insert in panel (a) shows a magnified view of the Pd nanoparticle pointed with a white arrow.

sponding to larger clusters or nanoparticles with a metallic character (Pd $3d_{5/2}$ and Pd $3d_{3/2}$ at 335.7 and 341.1 eV, respectively), which is more abundant as the Pd content increases.

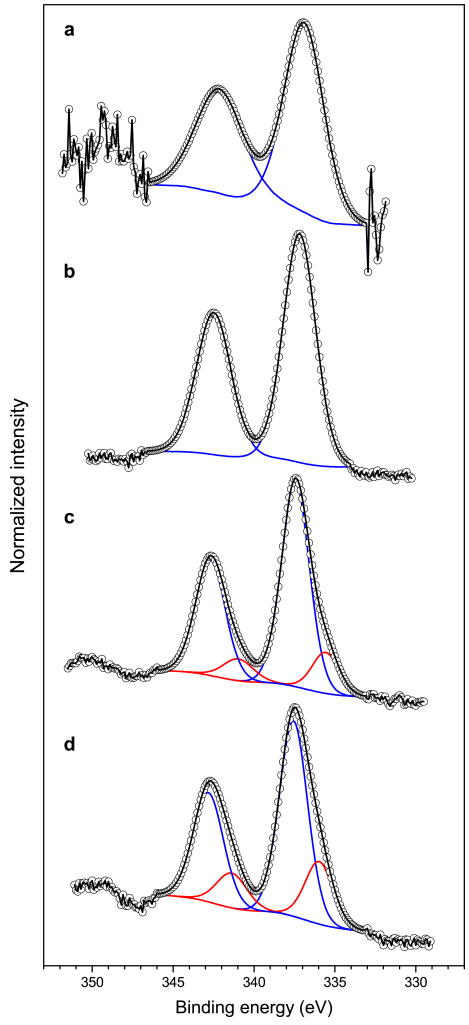

Fig. 4 XPS of samples 1-4. (a,b) The binding energies recorded in samples 1 and 2 are typical for ionic Pd and small Pd nanoclusters. (c,d) An additional component (in red) corresponding to larger clusters or nanoparticles with a metallic character is observed for the XP spectra of samples 3 and 4, respectively.

The catalytic performance of our catalysts is shown in Table 1 along with other representative examples in the literature. Surprisingly, the use of sample 1 –constituted uniquely by Pd SACs– did not catalyse the reaction at all even increasing both the reaction time and temperature. In contrast, sample 2 gave extraordinary results. The TOF obtained in mild reaction conditions was 5891 h^{-1}, and by increasing the temperature to 60°C an exceptional TOF of 13724 h^{-1} was achieved. Samples 3, 4 and 5 exhibited a systematic decrease of the catalytic activity. Figure 5 shows graphically these catalytic results at room temperature. This behaviour was reproduced with the 1-octene and cyclohexene substrates. In both cases, sample 1 was absolutely inactive while sample 2 permitted to obtain efficiently octane and cyclohexane, respectively (see ESI†). At this point, in order to explain the catalytic inactivity of the Pd SACs, it was important to discard the loss of accessibility to palladium through strong metal-support interaction (SMSI) effects. In this paper, the synthesis of the catalysts as well as the catalytic tests are conducted at room temperature; it is therefore very improbable that the SMSI effect occurs, given that it only takes place at high temperatures.[27] Besides, the HAADF-STEM images do not show any Pd surface decoration or

Table 1 Selected TOFs for the hydrogenation of styrene

Catalyst	Conditions	TOF (h^{-1})	Yield (%)[c]
Pd/Fe_3O_4 0.18 w% (sample 1)	3 bar, 20°C	0	0
Pd/Fe_3O_4 0.18 w% (sample 1)	10 bar, 75°C	0	0
Pd/Fe_3O_4 0.38 w% (sample 2)	3 bar, 20°C	5891 (7854)[d]	56
Pd/Fe_3O_4 0.38 w% (sample 2)	10 bar, 20°C	5448	52
Pd/Fe_3O_4 0.38 w% (sample 2)[a]	3 bar, 60°C	13724	65
Pd/Fe_3O_4 0.63 w% (sample 3)	3 bar, 20°C	4861 (10567)[d]	76
Pd/Fe_3O_4 0.90 w% (sample 4)	3 bar, 20°C	3687 (8379)[d]	83
Pd/Fe_3O_4 3.48 w% (sample 5)[b]	3 bar, 20°C	2605 (9303)[d]	75
Pd/microgel[21]	10 bar, 25°C	4800	
Pd NPs[22]	21 bar, 50°C	7704	
Pd/polymer[23]	1 bar, 35°C	1449	
Pd(II)/polymer[24]	1 bar, 25°C	766	
Pd/MOF[25]	1 bar, 35°C	703	
Pd/PEG[26]	1 bar, 25°C	660	
Pd/C[24]	1 bar, 25°C	377	

Turnover frequency, TOF = [mol of ethylbenzene/mol of Pd]/time(h). (a) Double styrene amount added (22.6 mmol). (b) Triple styrene amount added (33.9 mmol). (c) Yield after 1h of reaction. (d) TOF based on the palladium surface atoms.

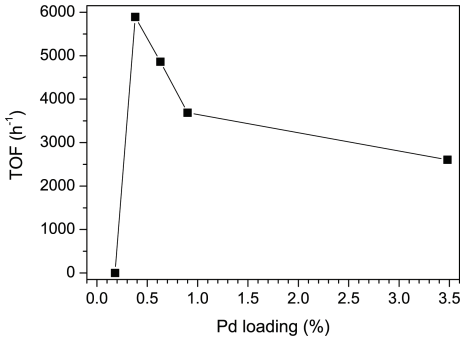

Fig. 5 TOF values obtained at rom temperature for the hydrogenation of styrene as a function of the Pd content.

encapsulation by the metal oxide support and, on the other hand, the catalytic performance of samples 2-5 is not altered after successive catalytic runs, thus, indicating that the accessibility of Pd is maintained after reaction (see below). The radically different catalytic behaviour between the Pd SACs and the small clusters can probably be attributed to the positive charge of the Pd SACs, as shown in the XPS spectra and confirmed by a good number of metal SACs reported up to now. Thus, the positive Pd atoms (or better, ions) are reluctant to be oxidized, preventing the formation of dihydride species, which is the first step for hydrogenation processes. Besides, all catalysts remained fully active during five complete cycles without apparent loss of activity. In addition to this, the HAADF-STEM images of the starting nanoparticles and those resulting from the second reaction cycle do not show appreciable differences (Fig. 2c and d) indicating a strong Pd-magnetite interaction.

The potential leach of Pd during the hydrogenation reaction was investigated. The magnetic nanoparticles were separated by an external magnet after one hour of reaction and the resulting solution was maintained reacting with hydrogen one additional hour. The analysis of the solution showed that the reaction did not progress. In good accord with this, no Pd was found in the final solution by ICPoes.

In conclusion, we have synthesized and characterized a sample constituted by single Pd atoms (0.18% weight) uniformly dispersed on the surface of magnetite nanoparticles that do not show any catalytic activity in the hydrogenation of alkenes. Remarkably, the Pd SACs seem to be strongly anchored onto the magnetite surface given that no Pd SACs aggregation occurs during the hydrogenation process, even at 80°C. Outstandingly, a sample (0.38% weight) with Pd nanoclusters in the range of 0.9-1.5 nm along with a few SACs was extremely active overcoming the best reported TOFs. Finally, samples with higher Pd loading constituted by larger Pd nanoparticles were catalytically less efficient.

This work was financially supported by the MICINN (projects CTQ2012-31335 and CTQ2010-15292). J. L. is a Serra Húnter Fellow and is grateful to the ICREA Academia program. Access to the TEM facilities at IBM Research-Zurich, Switzerland, under the IBM/Empa Master Joint Development Agreement is gratefully acknowledged.

References

1 J. Zhang, X. Liu, X. Guo, S. Wu and S. Wang, *Chem. - Eur. J.*, 2010, **16**, 8108–8116.
2 D. Wang and D. Astruc, *Chem. Rev.*, 2014, **114**, 6949–6985.
3 M. B. Gawande, P. S. Branco and R. S. Varma, *Chem. Soc. Rev.*, 2013, **42**, 3371–3393.
4 M. Haruta, *Catal. Today*, 1997, **36**, 153–166.
5 Y. Lei, F. Mehmood, S. Lee, J. Greeley, B. Lee, S. Seifert, R. E. Winans, J. W. Elam, R. J. Meyer, P. C. Redfern, D. Teschner, R. Schloegl, M. J. Pellin, L. A. Curtiss and S. Vajda, *Science*, 2010, **328**, 224–228.
6 B. Qiao, A. Wang, X. Yang, L. F. Allard, Z. Jiang, Y. Cui, J. Liu, J. Li and T. Zhang, *Nature Chem.*, 2011, **3**, 634–641.
7 M. Moses-DeBusk, M. Yoon, L. F. Allard, D. R. Mullins, X. Y. Z. Wu, G. Veith, G. M. Stocks and C. K. Narula, *J. Am. Chem. Soc.*, 2013, **135**, 12634–12645.
8 X. Guo, G. Fang, G. Li, H. Ma, H. Fan, L. Yu, C. Ma, X. Wu, D. Deng, M. Wei, D. Tan, R. Si, S. Zhang, J. Li, L. Sun, Z. Tang, X. Pan and X. Bao, *Science*, 2014, **334**, 616–619.
9 J. H. Kwak, L. Kovarik and J. Szanyi, *ACS Catal.*, 2013, **3**, 2094–2100.
10 L. Zhang, A. Wang, J. T. Miller, X. Liu, X. Yang, W. Wang, L. Li, Y. Huang, C.-Y. Mou and T. Zhang, *ACS Catal.*, 2014, **4**, 1546–1553.
11 Z.-Y. Li, Z. Yuan, X.-N. Li, Y.-X. Zhao and S.-G. He, *J. Am. Chem. Soc.*, 2014, **136**, 14307–14313.
12 A. Corma, P. Concepcion, M. Boronat, M. J. Sabater, J. Navas, M. J. Yacaman, E. Larios, A. Posadas, M. A. Lopez-Quintela, D. Buceta, E. Mendoza, G. Guilera and A. Mayoral, *Nature Chem.*, 2013, **5**, 775–781.
13 E. J. Peterson, A. T. D. L. Riva, S. Lin, R. S. Johnson, H. Guo, J. T. Miller, J. H. Kwak, C. H. F. Peden, B. Kiefer, L. F. Allard, F. H. Ribeiro and A. K. Datye, *Nat. Commun.*, 2014, **5**, 4885.
14 G. Vile, D. Albani, M. Nachtegaal, Z. Chen, D. Dontsova, M. Antonietti, N. Lopez and J. Perez-Ramirez, *Angew. Chem., Int. Ed.*, 2015, **54**, 11265–11269.
15 S. F. J. Hackett, R. M. Brydson, M. H. Gass, I. Harvey, A. D. Newman, K. Wilson and A. F. Lee, *Angew. Chem., Int. Ed.*, 2007, **46**, 8593–8596.
16 H. Yan, H. Cheng, H. Yi, Y. Lin, T. Yao, C. Wang, J. Li, S. Wei and J. Lu, *J. Am. Chem. Soc.*, 2015, **137**, 10484–10487.
17 G. Kyriakou, M. B. Boucher, A. D. Jewell, E. A. Lewis, T. J. Lawton, A. E. Baber, H. L. Tierney, M. Flytzani-Stephanopoulos and E. C. H. Sykes, *Science*, 2012, **335**, 1209–1212.
18 L. M. Rossi, I. M. Nangoi and N. J. S. Costa, *Inorg. Chem.*, 2009, **48**, 4640–4642.
19 F. Gonzalez de Rivera, I. Angurell, M. D. Rossell, R. Erni, J. Llorca, N. J. Divins, G. Muller, M. Seco and O. Rossell, *Chem. - Eur. J.*, 2013, **19**, 11963–11974.
20 K. McEleney, C. M. Crudden and J. H. Horton, *J. Phys. Chem. C*, 2009, **113**, 1901–1907.
21 Y. Zhang, X.-Y. Quek, L. Wu, Y. Guan and E. J. Hensen, *J. Mol. Catal. A: Chem.*, 2013, **379**, 53–58.
22 C. H. Yen, H.-H. Wei, H.-W. Lin and C.-S. Tan, *Appl. Organomet. Chem.*, 2012, **26**, 736–742.
23 Y. Lan, M. Zhang, W. Zhang and L. Yang, *Chem. - Eur. J.*, 2009, **15**, 3670–3673.
24 S. M. Islam, A. S. Roy, P. Mondal and N. Salam, *Appl. Organomet. Chem.*, 2012, **26**, 625–634.
25 Y. Pan, D. Ma, H. Liu, H. Wu, D. He and Y. Li, *J. Mater. Chem.*, 2012, **22**, 10834–10839.
26 F. A. Harraz, S. E. El-Hout, H. M. Killa and I. A. Ibrahim, *J. Catal.*, 2012, **286**, 184–192.
27 R. Naumann d´Alnoncourt, M. Friedrich, E. Kunkes, D. Rosenthal, F. Girgsdies, B. Zhang, L. Shao, M. Schuster, M. Behrens and R. Schlögl, *J. Catal.*, 2014, **317**, 220–228.